Measurement of the absolute wavefront curvature radius in a heterodyne interferometer

Gerald Hechenblaikner

EADS Astrium, Friedrichshafen, Germany (Gerald.Hechenblaikner@astrium.eads.net)

Received June 22, 2010; revised July 28, 2010; accepted July 29, 2010;
posted August 6, 2010 (Doc. ID 130495); published August 26, 2010

We present an analytical derivation of the coupling parameter relating the angle between two interfering beams in a heterodyne interferometer to the differential phase signals detected by a quadrant photodiode. This technique, also referred to as differential wavefront sensing, is commonly used in space-based gravitational wave detectors to determine the attitude of a test mass in one of the interferometer arms from the quadrant diode signals. Successive approximations to the analytical expression are made to simplify the investigation of parameter dependencies. Motivated by our findings, we propose what we believe to be a new measurement method to accurately determine the absolute wavefront curvature of a single measurement beam. We also investigate the change in the coupling parameter when the interferometer "test mirror" is moved from its nominal position, an effect which mediates the coupling of mirror displacement noise into differential phase measurements.

OCIS codes: 040.2840, 010.7350, 120.3940, 120.3180, 120.4640, 120.2650.

1. INTRODUCTION

In applications of optical metrology and instruments it is important to characterize not only the intensity but also the phase distribution of the beams propagating through the system. Wavefront sensing [1] that is the measurement and characterization of the optical wavefront also lies at the heart of adaptive optics [2], where one tries to compensate a wavefront aberration or mismatch of wavefront curvature [3] through iterative adjustment of corrective optical elements. The wavefront may also be used as a probe of the surface roughness and curvature of an optical element from which the probe beam is reflected. Common tools for wavefront sensing are the Hartmann–Shack sensor, which allows the reconstruction of the complete waveform from gradient and Laplacian data [4], or phase shifting interferometry [5]. In [6] a special charge-coupled device (CCD) camera has been developed to determine the relative wavefront over the CCD pixel-grid between two interfering beams in a heterodyne interferometer.

In this paper we propose a novel method of determining the absolute wavefront curvature of one of the interfering beams in a heterodyne interferometer without using a sophisticated additional equipment. Optical heterodyne interferometers find numerous applications in the field of high-precision metrology where distance variations are measured with sub-wavelength precision over a large dynamic range [7,8]. The heterodyne interferometers used in gravitational wave detection technology under current development [9–14] are used to precisely determine not only the position of a test mass but also its attitude to picometer and nanoradian precisions, respectively. The test mass attitude is determined from differential wavefront signals. In differential wavefront sensing (DWS) the relative angle between two interfering beams is inferred from the differential phase across the beam (see, e.g., [15]). The latter is usually obtained from the signals detected by the two halves of a photodiode. The great sensitivity of DWS coupled with its simple and practical implementation has made it the method of choice for attitude measurements in gravitational wave detectors.

This paper is structured as follows: We first derive an analytical expression for the coupling factor relating the attitude of a test mirror to the detected DWS signals. Starting from this expression we make a series of successive approximations which allow us to gain more insight into the beam parameter dependencies of the coupling factor. Based on our findings we propose a novel method of directly measuring the absolute wavefront curvature of the measurement beam; further image processing or data analysis is not required. We then investigate the dependency of the coupling parameter on translational movements along the optical path axis of the test mirror. These results are used to discuss the coupling of a longitudinal mirror-jitter into angular phase measurements in a parameter regime typical for space-borne heterodyne interferometers.

2. EXPERIMENTAL SCHEMATIC

A simplified schematic of a heterodyne interferometer is depicted in Fig. 1. The output of a laser is split into two beams, termed "reference" and "measurement" beams. The two beams are frequency-shifted relative to another by the heterodyne frequency f_{het} in the following acousto-optic-modulators AOM1 and AOM2. To clean up the beam profile the beams are then transmitted through optical fibers and fiber injectors onto the optical bench. There the measurement beam is following a path where it is reflected from two rotatable mirrors before being recombined with the reference beam on the recombination beam splitter. The interference pattern on the photodiode is

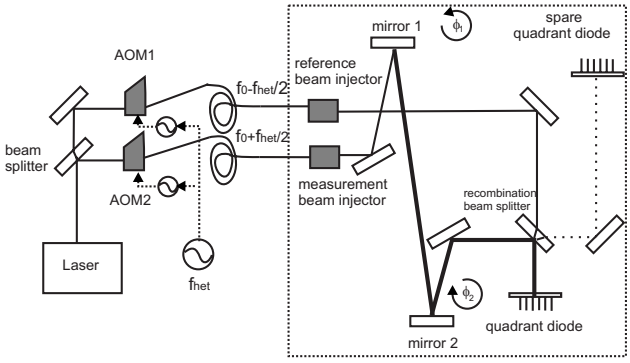

Fig. 1. Experimental setup to measure the absolute curvature of the measurement beam wavefront. Mirrors 1 and 2 are successively rotated in the opposite sense of rotation. A thick line is printed to indicate the lever arm from mirror 1 to the photodiode. The path to the spare photodiode is printed as a dotted line.

beating with the heterodyne frequency f_{het} and its phase is detected and measured by the two halves of a quadrant photodiode and a phase-meter.

3. ANALYTICAL DERIVATION OF THE DWS COUPLING PARAMETER

In this section we derive an analytical expression for the differential phase of the interference pattern detected by the quadrants of the photodiode. The amplitude of a Gaussian beam propagating along the z-direction beam is given by the following expression:

$$A = \frac{1}{w(z)}\sqrt{\frac{2}{\pi}}e^{-(x^2+y^2)/w^2(z)}e^{ik(x^2+y^2)/(2R)}e^{ikz}, \tag{1}$$

where the beam waist $w(z)$ and the beam radius of curvature $R(z)$ at position z are given in terms of the beam waist w_0 and the Rayleigh range $z_R=\pi w_0^2/\lambda$ by

$$w^2(z) = w_0^2\left(1+\frac{z^2}{z_R^2}\right),$$

$$R(z) = z\left(1+\frac{z_R^2}{z^2}\right). \tag{2}$$

We consider the case where two beams, the measurement and the reference beams, are interfering on a quadrant photodiode, as commonly used in interferometry, and calculate the differential phase in the horizontal direction (analog for the vertical direction).

The two beam amplitudes are given in their respective reference frames by

$$A_r = C_r e^{-(x^2+y^2)/w_r^2(z)}e^{ik(x^2+y^2)/2R_r(z)}e^{ikz},$$

$$A_m = C_m e^{-(\tilde{x}^2+\tilde{y}^2)/w_m^2(\tilde{z})}e^{ik(\tilde{x}^2+\tilde{y}^2)/2R_m(\tilde{z})}e^{ik\tilde{z}}, \tag{3}$$

where the constants $C=w^{-1}(z)(2/\pi)^{1/2}$ have been introduced for convenience. They intentionally are omitted from this point on as they have no impact on phase-differences and cancel out. The two beams propagate along the z-axis of their respective reference frames. For simplicity and without loss of generality we assume that the reference beam is centered in the frame of the quadrant diode ($x=0$), but the center of the measurement beam is offset by a distance x_0. The profiles of the two beams on the interference plane and their respective reference frames are depicted in Fig. 2.

The reference frame of the measurement beam $(\tilde{x},\tilde{y},\tilde{z})$ is obtained from the reference frame of the reference beam through a simple rotation and a translation along the x-axis:

$$\begin{pmatrix}\tilde{x}\\ \tilde{y}\\ \tilde{z}\end{pmatrix} = \begin{pmatrix}\cos\varphi & 0 & -\sin\varphi\\ 0 & 1 & 0\\ \sin\varphi & 0 & \cos\varphi\end{pmatrix}\begin{pmatrix}x\\ y\\ z\end{pmatrix} - \begin{pmatrix}x_0\\ 0\\ 0\end{pmatrix}. \tag{4}$$

Assuming that the angle φ between the two beams is small (<1 mrad), we neglect terms of order φ^2 or higher and obtain an expression for the amplitude of the measurement beam in the coordinate frame of the reference beam:

$$A_m = e^{-[(x-x_o)^2+y^2]/w_m^2(z)}e^{ik[(x-x_o)^2+y^2]/2R_m(z)}e^{ikz}e^{ikx\varphi}. \tag{5}$$

Note that the photodiode quadrants act as integrators which average the amplitudes of the incident beams. We now calculate the average complex amplitude of the interference pattern on the left half of the quadrant diode which is centered at $z=0$:

$$\begin{aligned}F_{\mathrm{left}} &= \int_{-\infty}^{\infty}\mathrm{d}y\int_{-\infty}^{0}\mathrm{d}x A_r A_m^*\\ &= \int_{-\infty}^{\infty}\mathrm{d}y\{\cdots\}\int_{-\infty}^{0}\mathrm{d}x e^{-2x^2/w_{\mathrm{eff}}^2}e^{ik(x^2/2R_{\mathrm{rel}})}e^{-ikx\varphi(1-z_{tm}/R_m)}\\ &\quad\times e^{ikx(x_{0s}/R_m)},\end{aligned} \tag{6}$$

where the effective beam w_{eff}, the relative beam radius R_{rel}, the "lever-arm length" z_{tm}, and the static beam displacement x_{0s} were introduced as

$$\frac{2}{w_{\mathrm{eff}}^2} = \frac{1}{w_m^2}+\frac{1}{w_r^2},$$

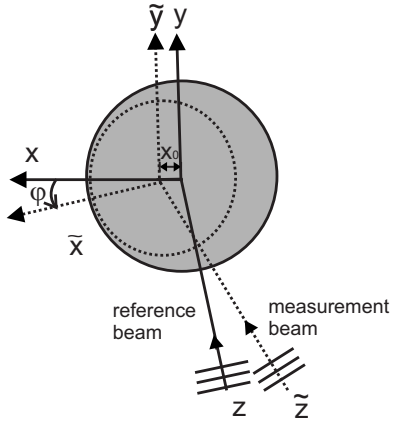

Fig. 2. Reference frames of the measurement beam (axes with tilde) and the reference beam (axes without tilde). The two beams propagate along $\tilde{z}$ and z, respectively, and interfere on the plane described by $z=0$.

$$\frac{1}{R_{\mathrm{rel}}} = \frac{1}{R_r} - \frac{1}{R_m},$$

$$x_0 = x_{0s} + \varphi z_{tm}. \tag{7}$$

Note that in Eq. (6) we neglected the beam displacement x_0 of the measurement beam in the expression for the intensity distribution $\exp(-2x^2/w_{\mathrm{eff}}^2)$. We have shown by comparison to the direct numerical integration of the exact expression that this is a very accurate approximation as long as the beam centers are not offset by more than half a beam waist. The overall distance between the two beams is the sum of a static distance (x_{0s}) when the two beams are parallel, and "the dynamically changing distance" (φz_{tm}), the origin of which is the deflection of the measurement beam from its parallel path by the angle φ at a distance z_{tm} from the plane of interference. Note that the distance between the mobile mirror and the interference plane is given by z_{tm}.

In Eq. (6) the terms in x and y separate and can therefore be integrated independently. As a consequence the integral in the vertical direction (y) cancels in the calculation of the DWS signal DWS_φ, which is defined as the differential phase between the left and the right halves of the quadrant diode:

$$DWS_\varphi = \arg\left(\frac{F_{\mathrm{left}}}{F_{\mathrm{right}}}\right) = \arg\left(\frac{\int_{-\infty}^{\infty} dy \int_{-\infty}^{0} dx A_r A_m^*}{\int_{-\infty}^{\infty} dy \int_{0}^{\infty} dx A_r A_m^*}\right) = \arg\left(\frac{\int_{-\infty}^{0} dx e^{-2x^2/w_{\mathrm{eff}}^2} e^{ik(x^2/2R_{\mathrm{rel}})} e^{-ikx\varphi(1-z_{tm}/R_m)} e^{ikx(x_{0s}/R_m)}}{\int_{0}^{\infty} dx e^{-2x^2/w_{\mathrm{eff}}^2} e^{ik(x^2/2R_{\mathrm{rel}})} e^{-ikx\varphi(1-z_{tm}/R_m)} e^{ikx(x_{0s}/R_m)}}\right). \tag{8}$$

In the derivation of Eq. (8) we made the simplifying assumption that the diode size is much larger than the beam diameter (one integral boundary extends to infinity) and that the "gap" between quadrants is very small (other integral boundary starts at zero). Considering the similarities of the terms in the numerator and denominator of Eq. (8), the derivation of DWS_φ is somewhat simplified and we obtain after some algebra

$$DWS_\varphi = \arg\left(\frac{1+i\alpha}{1-i\alpha}\right),$$

$$\alpha = \mathrm{erfi}\left(\frac{w_{\mathrm{eff}}}{2^{3/2}}\left(k\varphi\left(1-\frac{z_{tm}}{R_m}\right) - k\frac{x_{0s}}{R_m}\right)\sqrt{\frac{1+i\sigma}{1+\sigma^2}}\right),$$

$$\sigma = \frac{k w_{\mathrm{eff}}^2}{4R_{\mathrm{rel}}}, \tag{9}$$

where erfi is the imaginary error function defined by $\mathrm{erfi}(z) = -i\,\mathrm{erf}(iz)$. We now assume that the angle φ and the static displacement x_{0s} are very small and therefore only retain terms to first order in those parameters. In the expansion we neglect terms of second order or higher in φ and x_{0s} as well as any cross-terms. After expansion of the error function to first order in φ and x_{0s} and some lengthy algebra, we find

$$DWS_\varphi = \sqrt{\frac{2}{\pi}}\left(k w_{\mathrm{eff}}\varphi\left(1-\frac{z_{tm}}{R_m}\right) - k\frac{w_{\mathrm{eff}}x_{0s}}{R_m}\right)F(\sigma) + O(\varphi^2, x_{0s}^2),$$

$$F(\sigma) = \frac{1}{\sqrt{2}}\sqrt{\frac{1+\sqrt{1+\sigma^2}}{1+\sigma^2}}, \tag{10}$$

where $F(\sigma)$ in Eq. (10) depends on the nonlinearity parameter σ, which in turn depends on the diameter and the relative wavefront curvature of the two interfering beams. When σ goes toward zero, $F(\sigma)$ approaches 1. Typically, σ is quite small ($\sim 2\times 10^{-1}$), but can become significant under certain conditions. Therefore it should not be neglected. Expanding $F(\sigma)$ to second order in σ we obtain $F(\sigma) \approx (1 - 3/8\sigma^2)$. We shall now replace the angle φ between the two interfering beams with the angle ϕ of the rotatable mirror and consider that $2\phi = \varphi$. The coupling parameter D_ϕ^{m1} relates the differential tilt of mirror 1 ($\Delta\phi = \phi_1 - \phi_2$) to the differential change in the observed DWS signal; in other words it describes the linear slope with respect to ϕ of Eq. (10):

$$D_\phi^{m1} = \frac{d(DWS_\phi)}{d\phi} = \sqrt{2}\pi\frac{4w_{\mathrm{eff}}}{\lambda}\left(1-\frac{z_{tm}}{R_m}\right)F(\sigma). \tag{11}$$

We see from Eq. (11) that the coupling coefficient depends to first order on the effective beam waist w_{eff}, the measurement beam curvature R_m, and the lever-arm length z_{tm}. At higher orders, when $F(\sigma)$ becomes large, it also depends on the relative beam curvature R_{rel}.

Figure 3 shows the impact successive approximations have made, going from the exact result of Eq. (9) (solid line) to the approximate analytical result for small relative beam angles of Eq. (10) (dotted lines), up to the linear approximation for small nonlinearity parameter σ. We used the parameter values $R_{\mathrm{rel}} = 5.0$ m, $w_{\mathrm{eff}} = 8.8\times 10^{-4}$ m which are typical for a heterodyne interferometer such as the one in [9,10]. The approximations (dotted line) are given for values of $\phi = 200$ μrad, 350 μrad and 600 μrad, corresponding to values of the "small-angle parameter" $\gamma = k w_{\mathrm{eff}}\phi$ of $\gamma = 1.0$, 1.8, and 2.6, respectively. We also

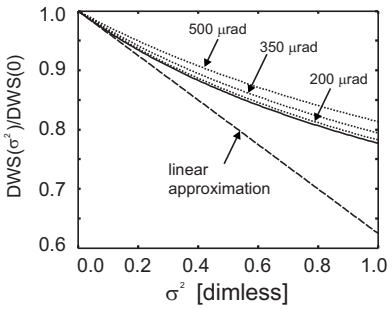

Fig. 3. DWS signals, normalized by their value for $\sigma^2=0$, are plotted against σ^2 while the value of $kw_{\text{eff}}\varphi$ is kept constant. The exact result is given by the solid line, the approximate results are given by the dotted lines, and the linearized approximate result is given by the dashed line.

checked the validity of Eq. (9) by comparison to the direct numerical integration of the interference integrals and found a perfect agreement.

We conclude that the approximation leading from Eq. (9) to Eq. (10) is a very good one for values of $\gamma \leq 1$. Equation (11) for the coupling parameter D_ϕ^{m1} provides the essential basis for the proposed measurements of the absolute beam curvature in the next section and it represents one major result of this article.

4. MEASURING THE ABSOLUTE WAVEFRONT CURVATURE

A. Measurement Approach

The dependency of Eq. (11) on the lever-arm length can be exploited by a setup such as the one depicted in Fig. 1. We propose to perform a measurement where at first mirror 1 is rotated by the differential angle $\Delta\phi$ and the corresponding difference in the DWS signal is measured. In the next step mirror 2 is rotated by exactly the same differential angle $\Delta\phi$ and the corresponding difference in the DWS signal is measured. The two measurements completely determine the coupling parameters D_ϕ^{m1}, D_ϕ^{m2}. Upon inspection of Eq. (11) we notice that all physical parameters determining the value of D_ϕ are identical in both test cases except for the lever-arm length. Taking the ratio β of the two coupling parameters we are therefore left with an expression that contains the radius of curvature of the measurement beam as the only unknown:

$$\beta = \frac{D_\phi^{m1}}{D_\phi^{m2}} = \frac{1 - z_{m1}/R_m}{1 - z_{m2}/R_m}. \tag{12}$$

Solving Eq. (12) for the radius of curvature we find

$$R_m = \frac{z_{m1} - \beta z_{m2}}{1 - \beta}. \tag{13}$$

We have therefore shown that through measurements of only two DWS-signal differences, when first mirror 1 and then mirror 2 are tilted, it is possible to determine the absolute wavefront curvature of the measurement beam. Such measurements are described in detail in [12]. The error of these measurements is discussed in the following subsection.

B. Error Analysis

The error in the ratio of coupling parameters (β) is given by

$$\Delta\beta = \frac{D_\phi^{m1}}{D_\phi^{m2}} \sqrt{\left(\frac{\Delta D_\phi^{m1}}{D_\phi^{m1}}\right)^2 + \left(\frac{\Delta D_\phi^{m2}}{D_\phi^{m2}}\right)^2}. \tag{14}$$

Considering an error in the coupling coefficients of $\Delta D_\phi \approx 0.03 D_\phi$, which is typical for measurements where the mirror tilt is accomplished by piezoelectric transducers with inherently large inaccuracies and hysteretic behavior, we obtain $\Delta\beta \approx \beta \times 0.05$ (see also [12]). Assuming typical values of $\beta = 2/3$, $R_m = 1.0$ m, and $z_{m1} = 0.5$ m and $z_{m2} = 0.25$ m, we find for the error ΔR_m of the radius of curvature

$$\Delta R_m = \frac{\Delta\beta}{1-\beta}(R_m - z_{m2}) = 0.08 \text{ m}. \tag{15}$$

The finite wavefront curvature affects a change in phase across the beam which is given by the complex exponent of Eq. (3). We find that the phase $\varphi(x)$ changes from the beam center to the edge of the waist by an amount of

$$\varphi(w) = \frac{kw^2}{2R_m} \approx \frac{2\pi}{3} \triangleq \frac{\lambda}{3}, \tag{16}$$

where we used a value of $w = 10^{-3}$ m for the beam waist and the wavelength of $\lambda = 1.064 \times 10^{-6}$ m.

From the error in the measurement of R_m [Eq. (15)] we find the error in the phase measurement:

$$\Delta\varphi(w) = \frac{kw^2}{2R_m}\frac{\Delta R_m}{R_m} \triangleq \frac{\lambda}{40}. \tag{17}$$

In other words, a measurement of the wavefront curvature with the accuracy given in Eq. (15) implies a phase measurement with the accuracy given in Eq. (17).

Note that the overall accuracy depends on the precision with which the coupling parameters D_ϕ are measured. Those in turn depend on the precision with which the dummy mirrors 1 and 2 can be reproducibly rotated by the differential angle $(\phi_1 - \phi_2)$. If we assume a perfect tilt precision, the measurement is only limited by the heterodyne phase-meter accuracy (typically better than 10^{-4} rad) which implies a resolution limit of $\Delta R_m \approx 2 \times 10^{-4}$ m.

C. Determining Other Beam Parameters

It is possible to determine all beam parameters *in situ*, i.e., from the setup described in Fig. 1 and without recourse to an additional test or measurement equipment. This simplifies any efforts and is useful in instruments where either tight confinement or handling restrictions do not allow the controlled insertion of measurement probes on multiple locations of the beam path. On the downside, due to the strong dependence of D_ϕ on the measurement rather than the reference beam parameters, the values for the reference beam parameters cannot be determined very accurately by the method suggested below, but it suffices to verify that the calculated parameters are consistent with expectations.

In total we have four unknowns, the two beam parameters for the measurement beam R_m, w_m and the two parameters for the reference beam, R_r, w_r, but with only two equations to solve for them. One of the unknowns, R_m, has already been calculated from the ratio of the two equations, which only leaves one independent equation. The waist of the measurement beam can be determined in a separate measurement by incrementally tilting mirror 1 and scanning the beam profile across the diode.

To find the beam parameters of the reference beam we revert to the full equation (11) for D_ϕ^{m1} and the analogous equation for D_ϕ^{m2}. Using the spare photodiode located in the other measurement arm after the recombination beam splitter (dotted line in Fig. 1), we obtain two more equations for $\hat{D}_\phi^{m1}$ and $\hat{D}_\phi^{m2}$ which denote the coupling parameters for mirrors 1 and 2 measured on the spare diode, respectively. The beam waists and curvature radii are different on this diode from those on the principal diode but they can be related to one another through Eq. (2). The wavefront curvature radius of the measurement beam can be found once more from the ratio of $\hat{D}_\phi^{m1}$ to $\hat{D}_\phi^{m2}$. Using an iterative simplex search method, the two reference beam parameters are easily found from the two independent equations for D_ϕ^{m1} and $\hat{D}_\phi^{m1}$. From a simulation which implements the setup in Fig. 1 and the measurements performed to determine the beam parameters, we find that the simulated measurement results match the input beam parameters with a sufficient accuracy.

5. POSITION DEPENDENCE OF THE COUPLING PARAMETERS AND NOISE COUPLING

Some parts of this section, especially the final paragraph, address specific sensitivity and alignment issues which are of importance in the design and usage of high-precision metrology systems such as those used in gravitational wave detectors [9,10,13,14]. In this section we investigate to which extent the coupling coefficients D_ϕ of Eq. (11) change with increasing lever-arm length, e.g., through the movement of mirror 1 or 2 along the axis of beam propagation (z-axis). As a consequence, the beam curvature, beam waist, and lever-arm length change on the interference plane so that all parameters which enter Eqs. (10) and (12), namely, w_{eff}, z_m, R_m, and R_{rel}, are affected. In the following discussion we consistently use the same beam parameters as in the previous sections: $R_m = 1.0$ m, $w_m = 1.0 \times 10^{-3}$ m and $R_r = 5/6$ m, $w_r = 0.8 \times 10^{-3}$ m. The lever-arm length is chosen to be $z_{m1} = 0.55$ m.

For an interferometer such as the one in Fig. 1 any test-mirror movement is accompanied by a parallel displacement of the measurement beam. A similar side-effect also occurs in the interferometers described in [9–12] where the beam is deflected from a test mirror at an acute angle of $\alpha = 4.5°$. A simplified schematic is given in Fig. 4, where we see that any change in the mirror position by the distance Δz implies a beam displacement by the distance $d = \Delta z \sin \alpha$. After moving the mirror the beam can either be left as it is, that is, displaced from its original position on the photodiode (dashed line), or the mirror is tilted slightly by the angle $\varepsilon = d/z_{tm}$ so that the displaced beam is guided back (dotted line) onto the center of the photodiode for optimal interference with the reference beam. For comparison the original beam path is given by the solid line.

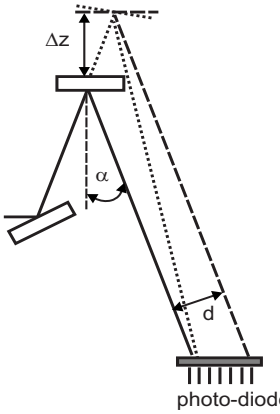

Fig. 4. Schematic of the interferometer described in [9]. The measurement beam is reflected from the test mirror at an angle α (solid line). When the mirror is moved the beam is displaced (dashed line). Its center on the photodiode can be aligned with its original position when the mirror is slightly tilted (dotted line).

The corresponding change in coupling coefficients, relative to the original value before the mirror was moved, is shown in Fig. 5. The coefficient decreases rapidly with increasing beam displacement (dashed line). If the beam displacement is compensated by increasing the angle between the measurement and reference beams (see Fig. 4), the coefficient decreases similarly fast (dotted line). If a polarizing interferometer is used, as in the gravitational wave-detector LISA (Laser Interferometer Space Antenna) [13,14] that is currently being built, the measurement beam incidence is normal to the test mirror and therefore no beam displacement occurs. There is only a very small increase in coupling constants due to the variation in beam width and wavefront curvature radius (solid line).

We find for the slopes $s_\phi = D_\phi^{-1}(z=0) \mathrm{d}D_\phi/\mathrm{d}z$ of the solid and dashed lines the values of $+0.3$ and -50 m^{-1}, respectively. The slope of the dashed line implies that the cou-

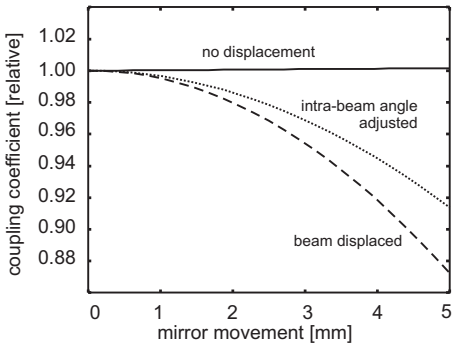

Fig. 5. Relative change in coupling coefficients D_ϕ when the test mirror in the setup of Fig. 4 is moved. The change in coefficients for increasing beam displacement is given by the dashed line. The dotted line is given for the case where the beam displacement is compensated by adjusting the test mirror and increasing the angle between reference and measurement beams. The solid line is given for the case of $\alpha = 0$ (no beam displacement).

pling coefficient changes by −5%/mm displacement, which stresses the importance of the correct alignment of the test mirror (in the actual detector it is a floating test mass) with the nominal interferometer position.

The slope of the curves in Fig. 5 also determines to what degree the longitudinal jitter of the test mass couples into the measurement noise of the attitude. The real physical (as opposed to the measurement sensor related) longitudinal displacement noise of the linear spectral density n_z couples into the angular noise of the linear spectral density n_ϕ as given by the following expression: $n_\phi = s_\phi \phi n_z$. We obtain $n_\phi = 2\times10^{-13}$ rad Hz$^{-1/2}$ for the realistically chosen parameters $n_z = 10\times10^{-12}$ m Hz$^{-1/2}$, $\phi = 400$ μrad, and $s_\phi = 50$ m^{-1}, which is 4 orders of magnitude below sensitivity requirements. In conclusion, even though an interferometer geometry where the measurement beam is reflected at an acute favors the coupling of longitudinal into angular noise, the expected effects are very small.

6. CONCLUSION

We derived an exact analytical expression for the differential phase across the interference pattern of two Gaussian beams as detected by a quadrant diode. Starting from the exact expression we successively introduced further approximations to simplify the discussion and gain a detailed understanding of the parameter interdependencies. All approximations were justified in detail by a numerical comparison to the exact expression.

Based on our findings we proposed a novel method to directly measure the absolute radius of wavefront curvature which requires two differential phase measurements following the successive rotation of two test mirrors. The measurement errors for this technique and its limiting accuracy were discussed in detail. We also studied the variation of the differential phase measurements as a function of the test-mirror movement and calculated the change in the coupling coefficient with increasing distance of the test mirror from its nominal location. A consequence of this effect, the coupling of the longitudinal displacement noise into the differential phase noise, was shown to be negligible in typical heterodyne interferometers.

ACKNOWLEDGMENTS

G. Hechenblaikner gratefully acknowledges stimulating discussions with David Robertson, University of Glasgow; Gudrun Wanner, Albert Einstein Institut in Hannover; and Vinzenz Wand, Rüdiger Gerndt, and Ulrich Johann, EADS Astrium Friedrichshafen. G. Hechenblaikner is grateful to I.C.Wijeyekoon from the R.B.C. for providing the encouragement, support, and means to write this paper.

REFERENCES

1. H. I. Campbell and A. H. Greenaway, "Wavefront sensing: From historical roots to state-of-the-art," in *Astronomy with High Contrast Imaging III: Instrumental Techniques, Modelling and Data Processing*, EAS Publications Series, M. Carbillet, ed. (EDP Sciences, 2006), Vol. 22, pp. 165–185.
2. H. W. Babcock, "The possibility of compensating astronomical seeing," Publ. Astron. Soc. Pac. **65**, 229–236 (1953).
3. F. Roddier, "Curvature sensing and compensation: a new concept in adaptive optics," Appl. Opt. **27**, 1223–1225 (1988).
4. S. Barbero, J. Rubinstein, and L. N. Thibos, "Wavefront sensing and reconstruction from gradient and Laplacian data measured with a Hartmann–Shack sensor," Opt. Lett. **31**, 1845–1847 (2006).
5. J. Millerd, N. Brock, J. Hayes, B. Kimbrough, M. Novak, M. North-Morris, and J. C. Wyant, "Modern approaches in phase measuring metrology," Proc. SPIE **5856**, 14–22 (2005).
6. F. Guzman Cervantes, G. Heinzel, A. F. García Marín, V. Wand, F. Steier, O. Jennrich, and K. Danzmann, "Real-time phase-front detector for heterodyne interferometers," Appl. Opt. **46**, 4541–4548 (2007).
7. C. M. Wu, S. T. Lin, and J. Fu, "Heterodyne interferometer with two spatially separated polarization beams for nanometrology," Opt. Quantum Electron. **34**, 1267–1276 (2002).
8. F. Zhao, "Picometer laser metrology for the Space Interferometry Mission," in *Conference on Lasers and Electro-Optics (CLEO)*, Vol. 96 of Trends in Optics and Photonics Series (Optical Society of America, 2004).
9. G. Heinzel, C. Braxmaier, R. Schilling, A. Ruediger, D. Robertson, M. te Plate, V. Wand, K. Arai, U. Johann, and K. Danzmann, "Interferometry for the LISA technology package (LTP) aboard SMART-2," Class. Quantum Grav. **20**, S153–S161 (2003).
10. D. Robertson, C. Killow, H. Ward, J. Hough, G. Heinzel, A. Garcia, V. Wand, U. Johann, and C. Braxmaier, "LTP interferometer—noise sources and performance," Class. Quantum Grav. **22**, S155–S163 (2005).
11. G. Heinzel, C. Braxmaier, M. Caldwell, K. Danzmann, F. Draaisma, A. F. Garcia Marin, J. Hough, O. Jennrich, U. Johann, C. Killow, K. Middleton, M. te Plate, D. Robertson, A. Ruediger, R. Schilling, F. Steier, V. Wand, and H. Ward, "Successful testing of the LISA Technology Package (LTP) interferometer engineering model," Class. Quantum Grav. **22**, S149–S154 (2005).
12. G. Hechenblaikner, R. Gerndt, U. Johann, P. Luetzow-Wentzky, V. Wand, H. Audley, K. Danzmann, A. Garcia-Marin, G. Heinzel, M. Nofrarias, and F. Steier, "Coupling characterization and noise studies of the Optical Metrology System on-board the LISA Pathfinder mission" (submitted to Appl. Opt.); preprint on arXiv:1006.2122.
13. D. A. Shaddock, "Space-based gravitational wave detection with LISA," Class. Quantum Grav. **25**, 114012 (2008).
14. D. Weise, P. Marenaci, P. Weimer, M. Berger, H. R. Schulte, P. Gath, and U. Johann, "Opto-mechanical architecture of the LISA instrument," in *Proceedings of the 7th International Conference on Space Optics (ICSO)*; www.icsoconference2008.com (2008).
15. H. Grote, G. Heinzel, A. Freise, S. Gossler, B. Wilke, H. Lueck, H. Ward, M. M. Casey, K. A. Strain, D. Robertson, J. Hough, and K. Danzmann, "Alignment control of GEO600," Class. Quantum Grav. **21**, S441–S449 (2004).